IOP Publishing | Institute of Physics and Engineering in Medicine Physiological Measurement

Physiol. Meas. **36** (2015) 2317–2333 doi:10.1088/0967-3334/36/11/2317

Respiratory rate derived from smartphone-camera-acquired pulse photoplethysmographic signals

Jesús Lázaro[1,2], Yunyoung Nam[3], Eduardo Gil[1,2], Pablo Laguna[1,2] and Ki H Chon[4]

[1] BSICoS Group, Aragón Institute of Engineering Research (I3A), IIS Aragón, Universidad de Zaragoza, 12, 50018, Zaragoza, Spain
[2] Centro de Investigación Biomédica en Red Bioingeniería, Biomateriales y Nanomedicina (CIBER-BBN), Zaragoza, Spain
[3] Department of Computer Science and Engineering, Soonchunhyang University, Asan 336–745, Korea
[4] Department of Biomedical Engineering, University of Connecticut, Storrs, CT 06269-3247, USA

E-mail: jlazarop@unizar.es, yynams@gmail.com and kchon@engr.uconn.edu

Received 24 April 2015, revised 16 August 2015
Accepted for publication 21 August 2015
Published 9 October 2015

Abstract

A method for deriving respiratory rate from smartphone-camera-acquired pulse photoplethysmographic (SCPPG) signal is presented. Our method exploits respiratory information by examining the pulse wave velocity and dispersion from the SCPPG waveform and we term these indices as the pulse width variability (PWV). A method to combine information from several derived respiration signals is also presented and it is used to combine PWV information with other methods such as pulse amplitude variability (PAV), pulse rate variability (PRV), and respiration-induced amplitude and frequency modulations (AM and FM) in SCPPG signals.

Evaluation is performed on a database containing SCPPG signals recorded from 30 subjects during controlled respiration experiments at rates from 0.2 to 0.6 Hz with an increment of 0.1 Hz, using three different devices: iPhone 4S, iPod 5, and HTC One M8. Results suggest that spontaneous respiratory rates (0.2–0.4 Hz) can be estimated from SCPPG signals by the PWV- and PRV-based methods with low relative error (median of order 0.5% and interquartile range of order 2.5%). The accuracy can be improved by combining PWV and PRV with other methods such as PAV, AM and/or FM methods. Combination of these methods yielded low relative error for normal respiratory rates, and

maintained good performance at higher rates (0.5–0.6 Hz) when using the iPhone 4S or iPod 5 devices.

Keywords: respiration, photoplethysmography, PPG, pulse width variability, PWV

(Some figures may appear in colour only in the online journal)

1. Introduction

Monitoring of respiration is usually performed by techniques such as spirometry, pneumography, and plethysmography. These techniques require cumbersome devices which are impractical in certain situations such as stress test or sleep studies (Bailón *et al* 2006b), and which may interfere with natural breathing. Thus, obtaining accurate respiratory information from comfortable non-invasive devices is a task of interest.

This paper is focused on deriving respiratory rate by using smartphone devices. This cannot fully replace spirometry which offers also information about respiratory-volume-related parameters. However, respiratory rate by itself is useful in several situations, e.g. it remains a sensitive clinical parameter in many pulmonary diseases (Krieger *et al* 1986) such as acute respiratory dysfunction (Gravelyn and Weg 1980). Impedance-pneumography-based techniques can be used when respiratory rate is the only respiratory information required since it is not designed to obtain other physiological parameters. These techniques are non-invasive and comfortable as they use only a pair of electrodes to measure the impedance changes in the chest. However, they often lead to unusable signals due to low signal-to-noise ratio and motion artifacts (Larsen *et al* 1984).

Many algorithms for deriving respiratory rate from comfortable non-invasive devices have been presented. Most of them use the electrocardiogram (ECG), exploiting variations of beat morphology and/or occurrence (Mason and Tarassenko 2001, Bailón *et al* 2006a, 2006b, Lázaro *et al* 2014a). There are methods based on other biomedical signals such as blood pressure (De Meersman *et al* 1996), photoplethysmographic (PPG) signals (Chon *et al* 2009, Lázaro *et al* 2013), and pulse transit time (Chua and Heneghan 2005), which require both ECG and PPG signals to derive respiratory rate.

The PPG signal is usually provided by a biomedical sensor called a pulse oximeter. It is composed of a light source which illuminates tissue (usually fingers, earlobes, or forehead) and a light detector which measures the reflected or transmitted light depending on its position, leading to a signal which is proportional to the blood volume. Deriving respiratory information from a PPG signal is particularly interesting, because pulse oximeters are very simple, economical, and comfortable to use. Furthermore, the pulse oximeter is widely adopted to monitor the peripheral oxygen saturation, which constitutes a very relevant parameter in the study of respiration. Thus, the pulse oximeter is a very valuable device in clinical settings.

Known methods for deriving respiratory rate from the PPG signal exploit variations on pulse morphology and/or occurrence. It is well known that respiration modulates heart rate (Hirsch and Bishop 1981) leading to a respiratory component in heart rate variability (Task Force 1996), which is also seen in pulse rate variability (PRV) since they are highly correlated (Gil *et al* 2010). Respiration also modulates the morphology of the PPG signal. Inspiration can lead to a reduction in tissue blood volume, and this lowers the amplitude of the PPG signal. This reduction in tissue blood volume is generated by two different mechanisms:

a reduction of cardiac output, and a reduction of intra-thoracic pressure (Meredith *et al* 2012). Variations in amplitude of the PPG signal have been used to obtain respiratory information (Johansson and Oberg 1999), and both heart and respiratory rates were extracted by methods based on empirical mode decomposition (Garde *et al* 2013), and based on correntropy spectral density (Garde *et al* 2014). There have been proposed other methods for obtaining respiratory rate based on the respiration-related amplitude and frequency modulations (AM and FM, respectively) in PPG signal (Chon *et al* 2009). Also, pulse width variability (PWV) have been proposed for deriving respiratory rate, either alone or in combination with other methods such as pulse amplitude variability (PAV) and PRV (Lázaro *et al* 2013). A time-frequency-coherence-based combination of PWV, PAV and PRV have been also proposed (Peláez-Coca *et al* 2013).

Smartphone devices can record PPG signals based on light emitted by flash and received by a camera (Jonathan and Leahy 2010, Grimaldi *et al* 2011). Smartphones are interesting devices in ambulatory scenarios due to significant advancements in the computational power which enables complex signal processing algorithms to be performed in real time. Certainly, built-in wireless communications feature of the smartphones facilitates ease of data transfer. These features make smartphones very valuable as 'take-anywhere' and easy-to-use physiological monitors (Scully *et al* 2012). Obtaining respiratory rates from smartphone devices would represent a simple and automated way for assisting hospital clinical staff who are currently trained to measure it by counting the number of breaths in a 15 or 30 s window (Pimentel *et al* 2014), making the process cumbersome and user-dependent. Other potential applications may include anxiety, fatigue or stress monitoring at home as respiratory rate is known to change in different anxiety/fatigue/stress situations (Marcora *et al* 2008, Niccolai *et al* 2009, Lackner *et al* 2011, Martinez *et al* 2015), especially if respiratory rate information is combined with other physiological information accessible in the PPG signal, such as pulse rate and its variability (Gil *et al* 2010) or blood pressure (Shaltis *et al* 2006).

It should be noted that, however, smartphone-camera-acquired-PPG (SCPPG) signal is more vulnerable to ambient-light interferences and variations in finger pressure over the sensor, making them in general noisier than the standard pulse oximeter sensor. Furthermore, their sampling rate is lower. Thus, deriving physiological information from SCPPG signals remains a more challenging situation than deriving it from conventional PPG signals, and the performance of known methods which have been tested with conventional PPG signals must be tested also with SCPPG signals.

In this paper, some PPG-based methods for deriving respiratory rate are studied with SCPPG signals. Concretely, the methods based on PRV, PAV, and PWV presented in (Lázaro *et al* 2013) are adapted to SCPPG signals. Furthermore, these methods are also combined with the AM- and FM-based methods presented in (Chon *et al* 2009). To the best of our knowledge, the PRV, PAV, and PWV-based methods have never been applied to SCPPG signals. In contrast, the AM- and FM-based methods have been tested with SCPPG signals in previous works (Scully *et al* 2012, Nam *et al* 2014). However, AM- and FM-based methods were neither combined with each other, nor with other methods. Note that a preliminary stage of the study described in this paper has been previously presented as a short conference paper (Lázaro *et al* 2014c). The present study is more comprehensive and new data are presented in this paper, including the study of several smartphone models with different hardware and form factor, which is relevant from the point of view of SCPPG signal acquisition.

2. Materials and methods

2.1. Data and signal preprocessing

We collected SCPPG data from 30 healthy subjects (22 men and eight women, between 20 and 26 years old) during controlled respiration experiments. Subjects were instructed to breathe at a constant rate according to a timed beeping sound, while sitting on a chair and placing the right index finger on the camera lens of the analyzed device. The data were collected for respiratory rates ranging from 0.2 to 0.6 Hz at an increment of 0.1 Hz, recording a total of 2 min of SCPPG signal for each subject, respiratory rate and device.

The SCPPG signals were recorded with 3 different smartphone devices: iPhone 4S, iPod 5, and HTC One M8. The signals were extracted from average of 50×50 pixel region of the green video signal at each frame. The reason for using only the green band is that there is high absorption by hemoglobin in the green range, and it has been demonstrated to give a stronger cardiac pulse signal than the red or blue bands during remote PPG imaging (Verkruysse *et al* 2008, Maeda *et al* 2011, Scully *et al* 2012, Matsumura *et al* 2014).

The sampling rate of SCPPG signals is variable due to internal processing load (Lee *et al* 2012), and it depends on the measuring device. The SCPPG signals were interpolated to a constant sampling rate of $f_S = 100$ Hz by using cubic splines. Furthermore, SCPPG signals are obtained as inverted PPG signals (Grimaldi *et al* 2011). Thus, the signals were inverted by multiplying by -1 to be used for further processing.

Next, the data were divided into 60 s-length data segments that were shifted every 10 s. A length of 60 s ensure at least 9 breaths of the lowest frequency eligible as respiratory rate in this work, which is 0.15 Hz. The baseline contamination was removed with a high-pass filter with a cutoff frequency of 0.3 Hz, and high frequency noise was considerably attenuated by a low-pass filter with a cutoff frequency of 35 Hz. Subsequently, the artifacts were automatically detected and removed by an algorithm based on Hjorth parameters described in (Gil *et al* 2008). Segments with 30% or more of the time containing artifactual signal were discarded.

2.2. Pulse-to-pulse methods

2.2.1. Significant points detection. SCPPG pulses apex points n_{A_i} were detected by an automatic PPG pulse detector based on a low-pass-differentiator filter and a time-varying threshold (Lázaro *et al* 2014b). Then, baseline point of the ith SCPPG pulse n_{B_i} was defined as the minimum previous to n_{A_i}:

$$n_{B_i} = \underset{n}{\operatorname{argmin}}\{x(n)\}, \quad n \in [n_{A_i} - 0.3f_S,\ n_{A_i}]\,, \tag{1}$$

where $x(n)$ denotes the SCPPG signal.

Another significant point of SCPPG pulses is the middle point n_{M_i}. It is defined as the point where $x(n)$ has reached half of the maximum pulse amplitude, as shown in equation (2). These n_{M_i} were taken as fiducial points for deriving the pulse rate, because they are located at the upslopes of the SCPPG pulses which represent a very abrupt zone of $x(n)$, so their location is robust against noise (Lázaro *et al* 2014b).

$$n_{M_i} = \underset{n}{\operatorname{argmin}}\left\{\left|x(n) - \frac{x(n_{A_i}) + x(n_{B_i})}{2}\right|\right\}, \quad n \in [n_{B_i},\ n_{A_i}]\,. \tag{2}$$

The SCPPG pulses width was measured by adapting the algorithm presented in (Lázaro *et al* 2013) for conventional PPG signals, based on pulse boundaries detection. Each pulse has two

boundaries: the onset n_{O_i} and the end n_{E_i}. They are detected by using a low-pass filtered first derivative of *x(n)*:

$$x'(n) = x_{LP}(n) - x_{LP}(n-1), \tag{3}$$

where $x_{LP}(n)$ is the low-pass filtered version of *x(n)*, using a cutoff frequency of f_c which was set to 2 Hz as shown in section 3.1.

The maximum upslope point n_{U_i} is defined as:

$$n_{U_i} = \underset{n}{\text{argmax}}\{x'(n)\}, \quad n \in [n_{A_i} - 0.4f_S,\ n_{A_i}]\,. \tag{4}$$

Note that the interval for searching n_{U_i} is larger than in (Lázaro *et al* 2013), where its length was 300 ms. This is done because SCPPG signals are reflected-light-based signals so their pulses are smoother and larger than those in transmitted-light-based PPG signals. Similarly, the interval in which the search for pulse wave onset n_{O_i} is also larger:

$$n_{O_i} = \underset{n}{\text{argmin}}\{\left|x'(n) - \eta x'(n_{U_i})\right|\},\ n \in \Omega_{O_i} = [n_{A_i} - 0.4f_S,\ n_{U_i}], \tag{5}$$

where $\eta x'(n_{U_i})$ represents a pulse-to-pulse varying threshold dependent on maximum upslope value of each pulse wave. The value of parameter η was set to 0.5 as shown in section 3.1.

Detection of pulse waves ends n_{E_i} was performed in a similar way as n_{O_i} but using maximum downslope n_{D_i} instead of n_{U_i} and $\Omega_{E_i} = [n_{D_i},\ n_{A_i} + 0.4f_S]$ instead of Ω_{O_i}.

2.2.2. Derived respiration signals. Three derived respiration (DR) signals were calculated by using pulse-to-pulse methods: PRV, PAV, and PWV. The DR signal based on PRV is obtained through the inverse interval function (Sörnmo and Laguna 2005):

$$d^u_{PRV}(n) = \sum_i f_S \frac{1}{n_{N_i} - n_{N_{i-1}}} \delta(n - n_{A_i}), \tag{6}$$

where superscript '*u*' denotes that the signal is unevenly sampled, and n_{N_i} are the arrival times of normal sinus pulses, which are determined from n_{M_i} after removing ectopic and miss-detected pulses using the method proposed in (Mateo and Laguna 2003).

On the other hand, the PAV- and PWV-based DR signals are defined as:

$$d^u_{PAV}(n) = \sum_i \left[x(n_{A_i}) - x(n_{B_i})\right] \delta(n - n_{A_i}) \tag{7}$$

$$d^u_{PWV}(n) = \sum_i \frac{1}{f_S} \left[n_{E_i} - n_{O_i}\right] \delta(n - n_{A_i}). \tag{8}$$

A median absolute deviation (MAD)-based outlier rejection rule described in (Bailón *et al* 2006a), and a 4 Hz evenly sampled version of each DR signal by cubic spline interpolation were applied. Then, these evenly sampled signals were filtered with a band-pass filter (0.15–0.7 Hz). The resulting signals are denoted without the superscript '*u*', e.g. $d_{PWV}(n)$ is the outlier-rejected, evenly sampled, band-pass filtered version of $d^u_{PWV}(n)$.

Figure 1 illustrates these pulse-to-pulse derived respiration signals.

2.3. Non-pulse-to-pulse methods

Amplitude and frequency modulation sequences, $d_{AM}(n)$ and $d_{FM}(n)$ respectively, were extracted from SCPPG signal as described in (Chon *et al* 2009). The amplitude and frequency

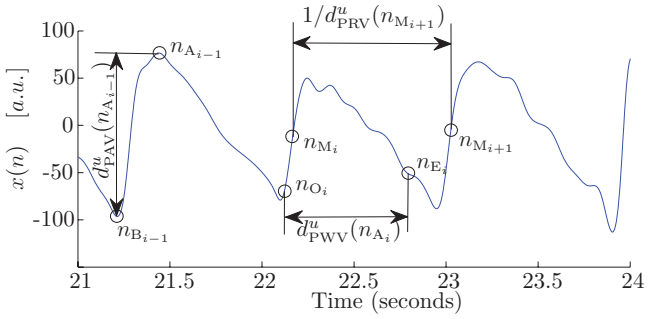

Figure 1. Pulse-to-pulse based derived respiration signals.

modulation sequences are extracted from a time-frequency (TF) spectrum obtained by the variable frequency complex demodulation (VFCDM) method (Wang *et al* 2006). The method for obtaining the VFCDM-based time-frequency spectrum can be divided into 2 steps: estimation of the dominant frequencies by fixed frequency complex demodulation (FFCDM), and subsequently applying VFCDM selecting only those dominant frequencies in order to improve the time-frequency resolution.

2.3.1. Fixed frequency complex demodulation. Let *x(t)* be a narrow-band oscillation:

$$x(t) = x_{DC}(t) + A(t)\cos(2\pi f_0 t + \phi(t)), \tag{9}$$

where f_0 is the center frequency, $A(t)$ is the instantaneous amplitude, $\phi(t)$ is the phase and $x_{DC}(t)$ is the dc component.

A(t) and $\phi(t)$ can be extracted for a given f_0 from *x(t)* by shifting f_0 to zero frequency multiplying it by $e^{-j2\pi f_0 t}$:

$$z(t) = x_{DC}(t)e^{-j2\pi f_0 t} + \frac{A(t)}{2}e^{-j\phi(t)} + \frac{A(t)}{2}e^{-j(4\pi f_0 t + \phi(t))}. \tag{10}$$

Then, the middle term of (10) can be obtained from $z(t)$, by applying a low-pass filter with a cutoff-frequency lower than f_0:

$$z_{LP}(t) = \frac{A(t)}{2}e^{-j\phi(t)}, \tag{11}$$

from which *A(t)* and $\phi(t)$ can be obtained as:

$$A(t) = 2|z_{LP}(t)| \tag{12}$$

$$\phi(t) = \tan^{-1}\left(\frac{\mathrm{Im}(z_{LP}(t))}{\mathrm{Re}(z_{LP}(t))}\right). \tag{13}$$

2.3.2. Variable frequency complex demodulation. Consider now that the modulating frequency varies as a function of time, $f_0(t)$. equation (9) can be rewritten as:

$$x(t) = x_{DC}(t) + A(t)\cos\left(\int_0^t 2\pi f_0(\tau)\mathrm{d}\tau + \phi(t)\right) \tag{14}$$

The frequency shift in (10) can be performed this time by multiplying x(t) by $e^{-j\int_0^t 2\pi f_0(\tau)\mathrm{d}\tau}$ obtaining:

$$z(t) = x_{\mathrm{DC}}(t)\mathrm{e}^{-j\int_0^t 2\pi f_0(\tau)\mathrm{d}\tau} + \frac{A(t)}{2}\mathrm{e}^{-j\phi(t)} + \frac{A(t)}{2}\mathrm{e}^{-j\left(\int_0^t 4\pi f_0(\tau)\mathrm{d}\tau + \phi(t)\right)}, \tag{15}$$

from which the middle term can be obtained similarly to the FFCDM case, i.e. by using a low-pass filter with a cut-off frequency lower than $f_0(t)$. Note that the expression of this term is the same than in the FFCDM case in (11) and thus, $A(t)$ and $\phi(t)$ can be obtained in the same way (see equations (12) and (13)). Then, the instantaneous frequency can be obtained as:

$$f(t) = f_0(t) + \frac{1}{2\pi}\frac{\mathrm{d}\phi(t)}{\mathrm{d}t}. \tag{16}$$

In this way, a time-frequency spectrum can be obtained by first applying FFCDM using a set of frequencies:

$$f_{0_k} = (k-1)(2f_\omega), \qquad k = 1, 2, \mathrm{int}\left(\frac{f_{\max}}{2f_\omega}\right). \tag{17}$$

where $2f_\omega$ is the bandwidth between successive center frequencies and $f_{\max}$ denotes the highest signal frequency.

The dominating frequencies $f_k(t)$ can be obtained from (16), and $A_k(t)$ can be obtained from (12). Subsequently, $f_k(t)$ were used as central frequencies for applying VFCDM refining the time-frequency resolution.

Parameter f_ω was set to 0.6 Hz. Further details are given in (Chon *et al* 2009).

2.3.3. Derived respiration signals. Once the VFCDM-based TF spectrum $S_{\mathrm{VFCDM}}(n,f)$ is computed, $d_{\mathrm{FM}}(n)$ is determined by extracting the frequency component that has the largest amplitude for each time point at the heart rate frequency band, since heart rate is considered the carrier wave:

$$d_{\mathrm{FM}}(n) = \underset{f\in\Omega_{\mathrm{HR}}}{\mathrm{argmax}}\{S_{\mathrm{VFCDM}}(n,f)\}, \tag{18}$$

where Ω_{HR} denotes the frequency band in which heart rate is expected. This band is defined by using the spectrum of the SCPPG signal $S_{\mathrm{SCPPG}}(f)$:

$$f_{\mathrm{HR}} = \underset{f}{\mathrm{argmax}}\{S_{\mathrm{SCPPG}}(f)\}, \quad f\in[0.5\mathrm{Hz},\ 2\mathrm{Hz}] \tag{19}$$

$$\Omega_{\mathrm{HR}} = [f_{\mathrm{HR}} - 0.2\mathrm{Hz},\ f_{\mathrm{HR}} + 0.3\mathrm{Hz}]. \tag{20}$$

A similar procedure is used for extracting the amplitude modulation:

$$d_{\mathrm{AM}}(n) = \max_f\{S_{\mathrm{VFCDM}}(n,f)\}, \quad f\in\Omega_{\mathrm{HR}}. \tag{21}$$

The values for parameters in these non-pulse-to-pulse methods were studied in previous works (Chon *et al* 2009, Scully *et al* 2012). The same processing applied to pulse-to-pulse-methods-based DR signals (section 2.2.2) was applied also to $d_{\mathrm{FM}}(n)$ and $d_{\mathrm{AM}}(n)$, i.e. a 4 Hz cubic spline interpolation followed by a band-pass filter (0.15–0.7 Hz). Figure 2 shows an example of DR signals studied in this paper.

2.4. Respiratory rate estimation

The respiratory rate is estimated from DR signals by an adaptation of the algorithm presented in (Lázaro *et al* 2013). It can combine information from several DR signals increasing the

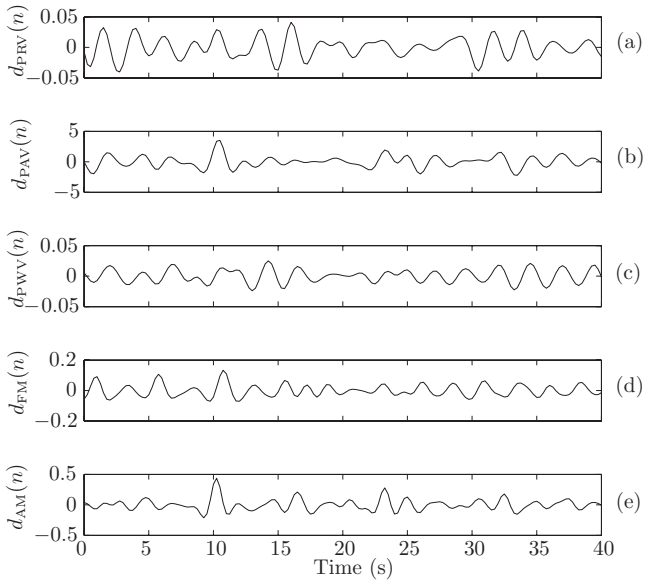

Figure 2. Example of derived respiration (DR) signals studied in this paper: $d_{PRV}(n)$ (a), $d_{PAV}(n)$ (b), $d_{PWV}(n)$ (c), $d_{FM}(n)$ (d), and $d_{AM}(n)$ (e). In this example, the subject was asked to maintain a respiratory rate of 0.4 Hz.

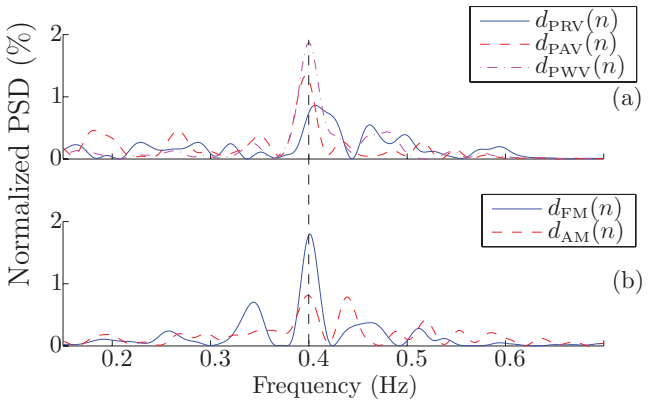

Figure 3. Example of normalized power spectrum densities (PSD) of derived respiration signals studied in this paper: $d_{PRV}(n)$, $d_{PAV}(n)$ and $d_{PWV}(n)$ (a), and $d_{FM}(n)$ and $d_{AM}(n)$ (b). In this example, the subject was asked to maintain a respiratory rate of 0.4 Hz.

robustness of the estimation. The algorithm can be divided in two phases: power spectrum density (PSD) estimation, and respiratory rate estimation.

First, the PSD of the jth DR signal $S_j(f)$ was estimated by applying a modified periodogram using a Hamming window. Then, the respiratory rate $\widehat{f}$ is the frequency at where the absolute maximum of the PSD is located, within the studied band [0.15, 0.7 Hz]. Figure 3 shows an example of normalized PSDs of DR signals studied in this paper.

Because $\widehat{f}$ is being estimated from more than one DR signals, their PSDs are 'peaked-condition averaged'; only those $S_j(f)$ which are sufficiently peaked take part in the averaging.

In this paper, 'peaked' denotes that a certain percentage (ξ) of PSD must be contained in an interval around its highest peak. In mathematical terms, 'peakness' of a PSD is defined as:

$$P_j = \frac{\int_{f_p(j)-0.05\text{Hz}}^{f_p(j)+0.05\text{Hz}} S_j(f)\mathrm{d}f}{\int_{0.15\text{Hz}}^{0.7\text{Hz}} S_j(f)\mathrm{d}f}, \tag{22}$$

where $f_p(j)$ denotes the highest peak within the studied band [0.15, 0.7 Hz] in the PSD of the jth DR signal.

In order to select those spectra that are sufficiently 'peaked', two different criteria were established: χ^{A} and χ^{B}. On the one hand, χ^{A} lets those spectra whose 'peakness' is greater than a fixed value take part in the average as shown in equation (14). On the other hand, χ^{B} compares the spectra of different DR signals, letting those spectra more peaked take part in the average, although all of them have passed the χ^{B} criterion as shown in equation (15).

$$\chi_j^{\mathrm{A}} = \begin{cases} 1, & P_j \geqslant \xi \\ 0, & \text{otherwise} \end{cases} \tag{23}$$

$$\chi_j^{\mathrm{B}} = \begin{cases} 1, & P_j \geqslant \max\limits_j\{P_j\} - \lambda \\ 0, & \text{otherwise} \end{cases}. \tag{24}$$

Then, the 'peak-conditioned' average is computed as:

$$\overline{S}(f) = \sum_j \chi_j^{\mathrm{A}}\chi_j^{\mathrm{B}} S_j(f). \tag{25}$$

Finally, $\widehat{f}$ is estimated as the frequency at which the absolute maximum of $\overline{S}(f)$ is located within the studied band [0.15, 0.7 Hz]:

$$\widehat{f} = \underset{f\in[0.15,\ 0.7]}{\operatorname{argmax}} \{\overline{S}(f)\}. \tag{26}$$

Respiratory rate was estimated from each one of the five DR signals separately, and from two combinations:

- $C_{\mathrm{PRV,PAV,PWV}}$: $d_{\mathrm{PRV}}(n)$, $d_{\mathrm{PAV}}(n)$ and $d_{\mathrm{PWV}}(n)$
- C_{ALL}: $d_{\mathrm{PRV}}(n)$, $d_{\mathrm{PAV}}(n)$, $d_{\mathrm{PWV}}(n)$, $d_{\mathrm{AM}}(n)$ and $d_{\mathrm{FM}}(n)$

3. Results

3.1. Pulse width parameters optimization

Optimal values for f_c and η parameters of pulse width measurement algorithm were obtained using a similar procedure to that used in (Lázaro *et al* 2013). Respiratory rate estimates from $d_{\mathrm{PWV}}(n)$ were computed for all the 323 possible combinations corresponding to $\eta \in [0, 0.8]$ with a step of 0.05, and $f_c \in [1, 10]$ Hz with a step of 0.5 Hz. The relative error of estimated respiratory rate was obtained as:

$$e_{\mathrm{R}} = \frac{\widehat{f} - f_{\mathrm{R}}}{f_{\mathrm{R}}} \times 100, \tag{27}$$

Table 1. Percentage of fragments excluded from the study due to the artifact and aliasing criteria.

	iPhone 4S		iPod 5		HTC One M8	
f_R (Hz)	Artifact	Aliasing	Artifact	Aliasing	Artifact	Aliasing
0.2	15.38%	0.00%	8.47%	0.00%	20.98%	0.00%
0.3	17.51%	0.00%	9.63%	0.00%	19.52%	0.00%
0.4	16.36%	0.00%	6.95%	0.00%	18.10%	0.00%
0.5	14.03%	1.36%	4.79%	6.38%	22.13%	0.00%
0.6	14.09%	24.55%	7.53%	35.48%	8.57%	15.71%

where f_R denotes the rate at which subject is requested to breathe.

Then, the values that minimized the mean of absolute value of e_R were obtained and chosen as optimal. These values were the same for the 3 studied devices: $\eta = 0.5$ and $f_c = 2$ Hz.

3.2. Respiratory rate estimation

The percentage of 60 s-length fragments excluded by the artifact criterion described in section 2.1 is shown in table 1. Note that aliasing problems may affect pulse-to-pulse methods, since respiratory information is obtained only at pulse occurrence. For this reason, fragments associated to a respiratory rate higher than the half mean pulse rate were excluded from the study. The percentage of fragments excluded by this criterion is also shown in table 1.

Relative error e_R was obtained for each studied DR signal and combination as defined in equation (27). Medians and interquartile ranges (IQR) obtained for e_R from different DR signals and combinations, for each f_R and device, are shown in table 2, and figure 4 shows them in a boxplot for a graphical visualization.

Furthermore, Kruskal-Wallis and the Bonferroni *t* test were used for analysis of differences of e_R for the different methods. The non-parametric Kruskal-Wallis statistical test was chosen because it was observed that e_R is not normal distributed, and the Bonferroni correction was applied in order to control the familywise error rate because multiple comparisons were performed. Table 3 shows those methods for which significant differences (p-value < 0.05) were observed.

4. Discussion

In this paper, two methods for deriving respiratory rate from SCPPG signals are presented. One of them combines information from pulse-to-pulse methods PRV, PAV and PWV, which were previously studied with conventional pulse oximeter PPG signals (Lázaro *et al* 2013). The other method presented in this paper uses the pulse-to-pulse methods in combination with non-pulse-to-pulse methods presented in (Chon *et al* 2009).

Deriving information from SCPPG signals is one challenging issue, since their low sampling rate and the ambient-light noise considerably affect their quality. In order to deal with this issue, an artifact detector (Gil *et al* 2008) was used to automatically exclude the artifactual fragments, which represents up to a 22.13% of the total fragments (HTC at $f_R = 0.5$ Hz).

The metronome frequency was used as reference for respiratory rate because a respiratory signal was not available when data were collected for the iPod 5 and HTC One M8 experiments. However, a respiratory signal from a respiration belt was available for 10 subjects in the iPhone 4S experiments and according to it, subjects breathed at the metronome respiratory

Table 2. Obtained medians and interquartile ranges (IQR) for e_R from different derived respiration signals and combinations, for each f_R and device.

f_R		iPhone 4S		iPod 5		HTC One M8	
(Hz)	DR Signal/Combination	Median	IQR	Median	IQR	Median	IQR
0.2	$d_{FM}(n)$	0.10%	2.44%	0.10%	0.00%	0.10%	2.44%
	$d_{AM}(n)$	0.10%	2.44%	0.10%	4.88%	0.10%	4.88%
	$d_{PRV}(n)$	0.10%	1.95%	0.10%	1.46%	0.10%	0.98%
	$d_{PAV}(n)$	0.10%	2.93%	0.10%	3.05%	1.07%	15.87%
	$d_{PWV}(n)$	0.10%	1.46%	0.10%	1.46%	0.10%	1.46%
	$C_{PRV.PAV.PWV}$	−0.39%	1.46%	−0.39%	0.98%	−0.39%	0.98%
	C_{ALL}	−0.39%	1.10%	−0.39%	0.98%	−0.39%	0.98%
0.3	$d_{FM}(n)$	0.91%	1.63%	−0.72%	1.63%	0.91%	18.31%
	$d_{AM}(n)$	−0.72%	3.66%	−0.72%	2.03%	−0.72%	3.26%
	$d_{PRV}(n)$	−0.07%	0.98%	−0.07%	1.06%	−0.07%	1.38%
	$d_{PAV}(n)$	−0.07%	1.95%	−0.39%	1.38%	−0.39%	2.36%
	$d_{PWV}(n)$	0.10%	0.98%	−0.07%	0.65%	−0.39%	1.63%
	$C_{PRV,PAV,PWV}$	0.91%	0.65%	−0.07%	0.98%	−0.07%	0.73%
	C_{ALL}	−0.07%	0.65%	−0.07%	0.98%	−0.07%	0.98%
0.4	$d_{FM}(n)$	0.10%	4.88%	0.10%	1.22%	0.10%	10.99%
	$d_{AM}(n)$	−2.34%	41.50%	−1.12%	36.62%	−1.12%	34.18%
	$d_{PRV}(n)$	−0.15%	1.22%	−0.15%	1.22%	0.10%	2.20%
	$d_{PAV}(n)$	−0.15%	3.17%	−0.39%	24.66%	−0.63%	15.38%
	$d_{PWV}(n)$	−0.15%	1.46%	−0.15%	1.22%	−0.15%	2.69%
	$C_{PRV.PAV.PWV}$	−0.15%	0.49%	−0.15%	0.73%	−0.15%	1.22%
	C_{ALL}	−0.15%	0.73%	−0.15%	0.73%	−0.15%	0.98%
0.5	$d_{FM}(n)$	−0.39%	3.17%	−0.39%	1.95%	−0.39%	11.72%
	$d_{AM}(n)$	−39.94%	55.91%	−39.45%	59.57%	−25.78%	56.64%
	$d_{PRV}(n)$	−0.20%	4.64%	−0.20%	1.17%	−0.20%	11.91%
	$d_{PAV}(n)$	−0.59%	44.14%	−0.39%	45.90%	−0.20%	26.56%
	$d_{PWV}(n)$	−0.20%	2.29%	0.00%	1.95%	−1.37%	39.06%
	$C_{PRV.PAV.PWV}$	−0.20%	0.78%	0.00%	0.78%	−0.20%	1.17%
	C_{ALL}	0.00%	0.98%	0.00%	0.78%	−0.20%	4.69%
0.6	$d_{FM}(n)$	−0.72%	50.05%	0.10%	46.39%	−3.97%	44.76%
	$d_{AM}(n)$	−49.95%	65.10%	−57.28%	66.73%	−37.74%	59.41%
	$d_{PRV}(n)$	−0.47%	36.42%	−0.23%	4.11%	−13.90%	56.32%
	$d_{PAV}(n)$	−2.99%	59.57%	−51.66%	69.42%	−31.64%	54.32%
	$d_{PWV}(n)$	−0.39%	32.63%	−0.07%	8.63%	−14.71%	48.50%
	$C_{PRV,PAV,PWV}$	−0.23%	2.40%	−0.07%	3.01%	−13.49%	54.57%
	C_{ALL}	−0.23%	2.12%	−0.07%	1.99%	−2.51%	37.64%

rate with an error of 0.12/1.01 mHz (median/interquartile range) which is accurate enough to consider the metronome frequency as a reference.

A high-pass filter with a cut-off frequency of 0.3 Hz was applied to SCPPG signals in order to significantly attenuate the baseline. Although in some situations respiration is below 0.3 Hz, this filter does not attenuate the respiration-induced variations in the amplitude of SCPPG signal exploited by some of the studied methods (PAV and AM). On one hand, PAV is based on pulse amplitude with respect to the baseline (see equation (7)). In this way, the information

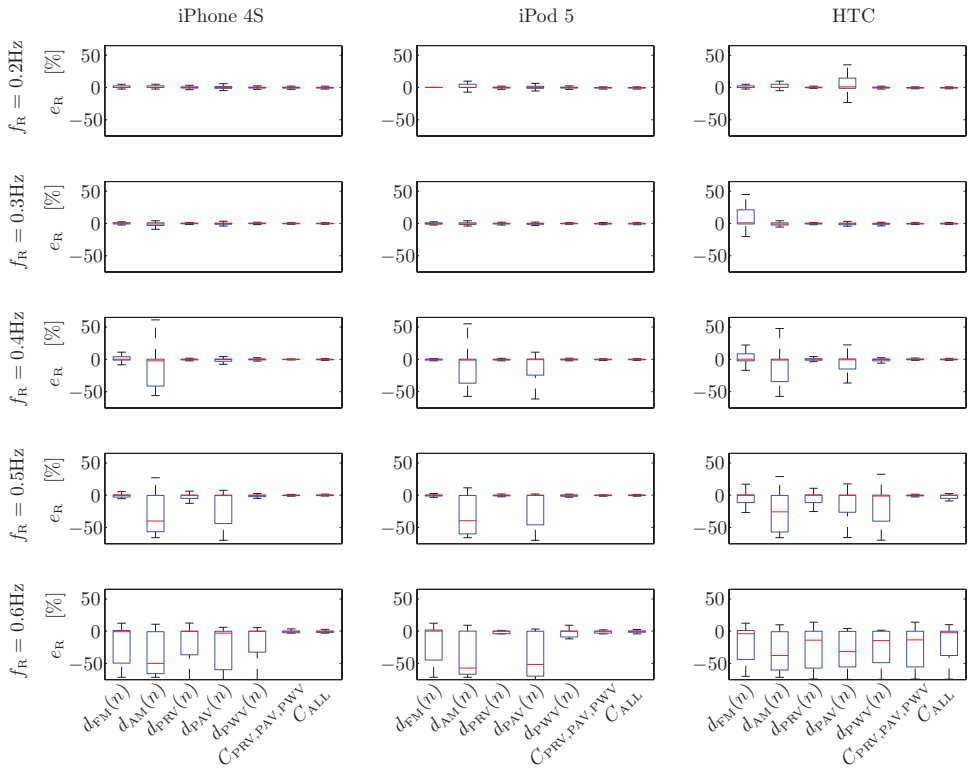

Figure 4. Boxplots of relative error e_R for the different methods, devices, and respiratory rates f_R.

Table 3. Pairs of methods for which significant differences were found in obtained e_R for different studied devices. Obtained e_R for normal range of spontaneous respiratory rate (0.2, 0.3 and 0.4 Hz) and for higher respiratory rates (0.5 and 0.6 Hz) were studied separately.

	$f_R \in \{0.2, 0.3, 0.4\}$ Hz	$f_R \in \{0.5, 0.6\}$Hz
iPhone 4S	{FM, AM}, {FM, PRV}, {FM, PAV}, {FM, PWV}, {FM. $C_{PRV,PAV,PWV}$}, {FM, C_{ALL}}, {AM, PWV}	{FM, AM}, {FM, PRV}, {AM, PRV}, {AM, PAV}, {AM, PWV}, {AM, $C_{PRV,PAV,PWV}$}, {AM, C_{ALL}}, {PRV, PAV}, {PAV, PWV}, {PAV, $C_{PRV,PAV,PWV}$}, {PAV, C_{ALL}}
iPod 5	{FM, AM}, {FM, PAV}, {AM, PRV}, {AM, PAV}, {AM, PWV}, {AM, $C_{PRV,PAV,PWV}$}, {AM. C_{ALL}}, {PRV, PAV}, {PAV, PWV}, {PAV, $C_{PRV,PAV,PWV}$}, {PAV, C_{ALL}}	{FM, AM}, {FM, PAV}, {AM, PRV}, {AM, PAV}, {AM, PWV}, {AM, $C_{PRV,PAV,PWV}$}, {AM, C_{ALL}} {PRV, PAV}, {PAV, PWV}, {PAV, $C_{PRV,PAV,PWV}$}. {PAV, C_{ALL}}
HTC	{FM, AM}, {FM, PRV}, {FM, PAV}, {FM, PWV}, {FM, $C_{PRV,PAV,PWV}$}, {FM, C_{ALL}}	{FM, AM}, {FM, PAV}, {FM, PWV}, {AM, PRV}, {AM, $C_{PRV,PAV,PWV}$}, {AM-C_{ALL}}

exploited by the PAV-based method is in the upwards slope of the pulses which correspond to a higher frequency. On the other hand, the AM method performs an amplitude demodulation considering the pulse rate to be the hypothetical carrier. Thus, the lower frequency exploited by the AM-based method is the pulse rate minus the respiratory rate, which is over 0.3 Hz.

In general, all studied methods obtained low median (of order 0.5%) and low IQR (of order 2.5%) of e_R until reaching a given respiratory rate, which depends on the method and on the device, e.g. $d_{PWV}(n)$ maintain good performance in e_R terms up to 0.5 Hz when using the iPhone 4S, and up to 0.4 Hz when using the HTC One M8. Similarly, in mathematical terms, no method was especially disadvantaged at higher respiratory rates. A possible reason for this observation is that the respiration-induced modulations on which DR signals are based (rate, amplitude and width) may have a less strong effect at higher respiratory rates. In the case of pulse rate, it is known that respiratory sinus arrhythmia (which modulates the heart rate and therefore the pulse rate) is reduced at high respiratory rates.

Results obtained for $d_{PWV}(n)$ were comparable to those obtained for $d_{PRV}(n)$ and better than for the other DR signals in general, obtaining low medians and IQR for e_R with f_R up to 0.4 Hz and even 0.5 Hz when using the iPhone 4S and iPod 5 devices. Occasionally, $d_{PWV}(n)$ and $d_{PRV}(n)$ obtained worse results (higher median/IQR for e_R) than another DR signal, such as $d_{FM}(n)$ when using the iPod 5 device with $f_R = 0.2$ Hz (0.10/0.00% versus −0.10/1.46%), or when using the HTC One M8 device with $f_R = 0.4$ Hz (−0.39/11.72% versus −0.20/11.91% and −1.37/39.06%).

Both combinations $C_{PRV,PAV,PWV}$ and C_{ALL} obtained low median (less than 0.5%) and IQRs (less than 2.5%) for e_R, in every case where at least one of the DR signals included in the combinations obtained low median and IQR for e_R, and even in some cases where none of the DR signals obtained low median and IQR for e_R. For instance, in the case of the iPhone 4S at $f_R = 0.6$ Hz, combinations obtained low median and IQR for e_R although DR signals obtained very high IQRs for e_R (up to 65.10%). Similarly, at $f_R = 0.5$ Hz, both combinations still obtained low median and IQR for e_R, even though in this case $d_{AM}(n)$ and $d_{PAV}(n)$ obtained high IQR (55.91% and 44.14%, respectively). These observations demonstrate the advantages of combining information.

C_{ALL} obtained similar results to $C_{PRV,PAV,PWV}$ in e_R terms, and significant statistical differences were not found between their associated e_R, for all devices either at normal ranges of spontaneous respiratory rate (0.2–0.4 Hz) or higher ones (0.5–0.6 Hz). These results suggest that C_{ALL} offers no advantages over $C_{PRV,PAV,PWV}$. A possible reason for this may be that respiratory information in $d_{AM}(n)$ and $d_{FM}(n)$ is mainly redundant with respiratory information in $d_{PAV}(n)$, $d_{PRV}(n)$ and/or $d_{PWV}(n)$. It is reasonable to believe that respiratory information in $d_{AM}(n)$ and $d_{PAV}(n)$ is redundant to a large extent, because they are based on similar effects: respiration-induced amplitude modulations, of the SCPPG signal in one case, and of pulses of SCPPG in the other one. A similar case occurs with $d_{FM}(n)$ and $d_{PRV}(n)$. Note that statistical differences were found in some cases between $d_{AM}(n)$ and $d_{PAV}(n)$ (iPhone 4S at 0.5–0.6 Hz and iPod 5 at both 0.2–0.4 Hz and 0.5–0.6 Hz) and between $d_{FM}(n)$ and $d_{PRV}(n)$ (iPhone 4S at both 0.2–0.4 Hz and 0.5–0.6 Hz, and HTC One M8 at 0.2–0.4 Hz). However before interpreting this observation it must be kept in mind that when a method fails in tracking respiration, the obtained e_R, especially when errors are big, has clear tendencies, see figure 4, so statistical differences in e_R should not be considered as an indicator of differences in the physiological origin of those respiratory-related modulations. When the statistical tests is repeated taking only those e_R between −15 and 15% (excluding outliers), no statistical differences are found between these methods in any device/respiratory rate condition, so corroborating results independence with the used methodology in respiratory frequency derivation when the methods

are able to catch the respiration. The differences are then in the different ability to provide meaningful estimation.

PPG-amplitude- and rate-based derived respiration signals present low frequency modulations below 0.15 Hz due to the Mayer wave related to sympathetic activity, which can be considered as noise from the point of view of deriving respiratory information. The power of these modulations is usually comparable or even higher than the respiration-related modulations, and this may confound respiratory rate estimation. Regarding the methods studied in this work, the low-frequency modulation affect to the AM and FM methods (Chon *et al* 2009) and to the PAV and PRV methods, but not to the PWV method according to (Lázaro *et al* 2013). For this reason, results for respiratory rates below 0.15 Hz are not provided in this work, in order to study if respiration-related modulations already studied in conventional PPG signals are also present in SCPPG signals, with independence of this kind of noise.

Those fragments associated with a f_R higher than half mean pulse rate were excluded, because the pulse-to-pulse methods would track an alias in such situations. This problem affects high f_R (0.5 and 0.6 Hz); e.g. for tracking a $f_R = 0.6$ Hz using pulse-to-pulse methods, it would be necessary to have a mean pulse rate of 1.2 Hz, i.e. 72 beats per min. However, a high f_R with a low pulse rate does not represent a realistic physiological situation. In such situations when the autonomic nervous system requires a high respiratory rate, it also requires a high heart rate which leads to a high pulse rate, e.g. during exercise. Nevertheless, some medications affect autonomic nervous system and may lead to non-physiological situations with a high f_R with a low pulse rate, e.g. beta-blockers. Furthermore, the physiological source of the respiration-related modulations in SCPPG signal exploited by the presented methods is the autonomic control over the cardiovascular system. In addition, PPG pulses morphology is affected by age, due to arterial stiffness. So age, arterial or autonomic nervous system diseases or medications interactions could affect results. This remains one limitation of this study because the methods have been evaluated only with recordings from healthy young people. Further studies must be elaborated to assess the performance of the presented methods over this kind of patients.

Another limitation of this study is that the inter-device variability for the same model of smartphones cannot be assessed because only one device per model has been tested. Slight differences in flashlight or camera lens may affect results. However, the form factor and so the distance between flashlight and camera lens, which is the most important signal-acquisition difference between different smartphone models, remains the same for devices of the same model. Nevertheless, if different models of smartphone would be wanted to be compared in the task of deriving respiratory rate, further studies using several devices for each model should be elaborated.

5. Conclusions

Results suggest that normal ranges of spontaneous respiratory rates (0.2–0.4 Hz) can be accurately estimated from smartphone-camera-acquired pulse photoplethysmographic signals based on pulse width variability or pulse rate variability with low e_R (median on the order of 0.5% and IQR on the order of 2.5%). The accuracy can be further improved by combining them with other methods such as pulse rate and amplitude variabilities, and amplitude and/or frequency modulations. Indeed, the combination of these methods resulted in lower e_R values within normal ranges of spontaneous respiratory rate, but with small degradation in its performance at higher rates (up to 0.5 Hz when using HTC One M8, and up to 0.6 Hz when using the iPhone 4S or iPod 5 devices).

These promising results suggest that accurate normal ranges of respiratory rates can be obtained from general people using only smartphones without using any external sensors. The methods could be extended to other models of smartphones or tablet devices, the only requirement is that these smartphones and tablets contain a video camera to image a fingertip pressed to it. As smartphones and tablets have become common, they meet the criteria of ready access and acceptance. Hence, our mobile phone/tablet approach has the potential to be widely-accepted by the general population and can facilitate the capability to measure some of the vital signs using only the subject's fingertip.

Acknowledgments

This work was supported in part by the US Army Medical Research and Materiel Command (USAMRMC) under Grant No. W81XWH-12-1-0541, by Universidad de Zaragoza under fellowship PIFUZ-2011-TEC-A-003, by Ministerio de Economía y Competitividad (MINECO), FEDER; under projects TIN2014-53567-R, TIN2013-42140-R, TEC2013-42140-R and FIS-PI12/00514, by CIBER de Bioingeniería, Biomateriales y Nanomedicina through Instituto de Salud Carlos III, and by Grupo Consolidado BSICoS (T96) from DGA (Aragón) and European Social Fund (EU). The computation was performed by the ICTS 'NANBIOSIS', more specifically by the High Performance Computing Unit of the CIBER in Bioengineering, Biomaterials & Nanomedicne (CIBER-BBN) at the University of Zaragoza.

References

Bailón R, Sörnmo L and Laguna P 2006a A robust method for ECG-based estimation of the respiratory frequency during stress testing *IEEE Trans. Biomed. Eng.* **53** 1273–85

Bailón R, Sörnmo L and Laguna P 2006b ECG-derived respiratory frequency estimation *Advanced Methods and Tools for ECG Data Analysis* ed G Clifford *et al* (Norwood, MA: Artech House Inc) pp 215–44

Chon K H, Dash S and Ju K 2009 Estimation of respiratory rate from photoplethysmogram data using time-frequency spectral estimation *IEEE Trans. Biomed. Eng.* **56** 2054–63

Chua C P and Heneghan C 2005 Pulse transit time-derived respiratory parameters and their variability across sleep stages *Proc. of the Ann. Int. Conf. IEEE Engineering Medical Biology Society* pp 6153–6

De Meersman R E, Zion A S, Teitelbaum S, Weir J P, Lieberman J and Downey J 1996 Deriving respiration from pulse wave: a new signal-processing technique *Am. J. Physiol.* **270** H1672–5

Garde A, Karlen W, Ansermino J M and Dumont G A 2014 Estimating respiratory and heart rates from the correntropy spectral density of the photoplethysmogram *PLoS ONE* **9** e86427

Garde A, Karlen W, Dehkordi P, Ansermino J and Dumont G 2013 Empirical mode decomposition for respiratory and heart rate estimation from the photoplethysmogram *Comput. Cardiol.* **2013** 799–802

Gil E, María Vergara J and Laguna P 2008 Detection of decreases in the amplitude fluctuation of pulse photoplethysmography signal as indication of obstructive sleep apnea syndrome in children *Biomed. Signal Process. Control* **3** 267–77

Gil E, Orini M, Bailón R, Vergara J M, Mainardi L and Laguna P 2010 Photoplethysmography pulse rate variability as a surrogate measurement of heart rate variability during non-stationary conditions *Physiol. Meas.* **31** 1271–90

Gravelyn T R and Weg J G 1980 Respiratory rate as an indicator of acute respiratory dysfunction *JAMA* **244** 1123–5

Grimaldi D, Kurylyak Y, Lamonaca F and Nastro A 2011 Photoplethysmography detection by smartphone's videocamera *Proc. of the IEEE 6th Int. Conf. on Intelligent Data Acquisition and Advanced Computing Systems (IDAACS)* vol 1 pp 488–91

Hirsch J A and Bishop B 1981 Respiratory sinus arrhythmia in humans: how breathing pattern modulates heart rate *Am. J. Physiol.* **241** H620–9

Johansson A and Oberg P A 1999 Estimation of respiratory volumes from the photoplethysmographic signal. Part I: experimental results *Med. Biol. Eng. Comput.* **37** 42–7

Jonathan E and Leahy M 2010 Investigating a smartphone imaging unit for photoplethysmography *Physiol. Meas.* **31** N79–83

Krieger B, Feinerman D, Zaron A and Bizousky F 1986 Continuous noninvasive monitoring of respiratory rate in critically ill patients *Chest* **90** 632–4

Lackner H K, Papousek I, Batzel J J, Roessler A, Scharfetter H and Hinghofer-Szalkay H 2011 Phase synchronization of hemodynamic variables and respiration during mental challenge *Int. J. Psychophysiol. Off. J. Int. Organ. Psychophysiol.* **79** 401–9

Larsen V H, Christensen P H, Oxhøj H and Brask T 1984 Impedance pneumography for long-term monitoring of respiration during sleep in adult males *Clin. Physiol. Oxford England* **4** 333–42

Lázaro J, Alcaine A, Romero D, Gil E, Laguna P, Pueyo E and Bailón R 2014a Electrocardiogram derived respiratory rate from QRS slopes and R-wave angle *Ann. Biomed. Eng.* **42** 2072–83

Lázaro J, Gil E, Bailón R, Mincholé A and Laguna P 2013 Deriving respiration from photoplethysmographic pulse width *Med. Biol. Eng. Comput.* **51** 233–42

Lázaro J, Gil E, Vergara J M and Laguna P 2014b Pulse rate variability analysis for discrimination of sleep-apnea-related decreases in the amplitude fluctuations of pulse photoplethysmographic signal in children *IEEE J. Biomed. Health Inform.* **18** 240–6

Lázaro J, Nam Y, Gil E, Laguna P and Chon K H 2014c Smartphone-camera-acquired pulse photoplethysmographic signal for deriving respiratory rate *Proc. of the 8th Conf. of the European Study Group on Cardiovascular Oscillations (ESGCO)* pp 121–2

Lee J, Reyes B A, McManus D D, Mathias O and Chon K H 2012 Atrial fibrillation detection using a smart phone *Proc. Ann. Int. Conf. IEEE EngineeringMedical Biology Society* pp 1177–80

Maeda Y, Sekine M and Tamura T 2011 The advantages of wearable green reflected photoplethysmography *J. Med. Syst.* **35** 829–34

Marcora S M, Bosio A and de Morree H M 2008 Locomotor muscle fatigue increases cardiorespiratory responses and reduces performance during intense cycling exercise independently from metabolic stress *Am. J. Physiol. Regul. Integr. Comp. Physiol.* **294** R874–83

Martinez J M, Garakani A, Aaronson C J and Gorman J M 2015 Heart rate and respiratory response to doxapram in patients with panic disorder *Psychiatry Res.* **227** 32–8

Mason C L and Tarassenko L 2001 Quantitative assessment of respiratory derivation algorithms *Proc. of the 23rd Ann. Int. Conf. of the IEEE Engineering in Medicine and Biology Society* vol 2 pp 1998–2001

Mateo J and Laguna P 2003 Analysis of heart rate variability in the presence of ectopic beats using the heart timing signal *IEEE Trans. Biomed. Eng.* **50** 334–43

Matsumura K, Rolfe P, Lee J and Yamakoshi T 2014 iPhone 4s photoplethysmography: which light color yields the most accurate heart rate and normalized pulse volume using the iPhysio meter application in the presence of motion artifact? *PloS One* **9** e91205

Meredith D J, Clifton D, Charlton P, Brooks J, Pugh C W and Tarassenko L 2012 Photoplethysmographic derivation of respiratory rate: a review of relevant physiology *J. Med. Eng. Technol.* **36** 1–7

Nam Y, Lee J and Chon K H 2014 Respiratory rate estimation from the built-in cameras of smartphones and tablets *Ann. Biomed. Eng.* **42** 885–98

Niccolai V, van Duinen M A and Griez E J 2009 Respiratory patterns in panic disorder reviewed: a focus on biological challenge tests *Acta Psychiatr. Scand.* **120** 167–77

Peláez-Coca M D, Orini M, Lázaro J, Bailón R and Gil E 2013 Cross time-frequency analysis for combining information of several sources: application to estimation of spontaneous respiratory rate from photoplethysmography *Comput. Math. Methods Med.* **2013** 631978

Pimentel M A F, Santos M D, Arteta C, Domingos J S, Maraci M A and Clifford G D 2014 Respiratory rate estimation from the oscillometric waveform obtained from a non-invasive cuff-based blood pressure device *Proc. Ann. Int. Conf. IEEE Engineering Medical Biology Society* pp 3821–4

Scully C G, Lee J, Meyer J, Gorbach A M, Granquist-Fraser D, Mendelson Y and Chon K H 2012 Physiological parameter monitoring from optical recordings with a mobile phone *IEEE Trans. Biomed. Eng.* **59** 303–6

Shaltis P A, Reisner A and Asada H H 2006 Wearable, cuff-less PPG-based blood pressure monitor with novel height sensor *Proc. Ann. Int. Conf. IEEE Engineering Medical Biology Society* pp 908–11

Sörnmo L and Laguna P 2005 ECG signal proccesing: heart rate variability *Bioelectrical Signal Processing in Cardiac and Neurological Applications* (Amsterdam: Elsevier)

Task Force of the European Society of Cardiology the North American Society of Pacing Electrophysiology 1996 Heart rate variability standards of measurement, physiological interpretation, and clinical use *Circulation* **93** 1043–65

Verkruysse W, Svaasand L O and Nelson J S 2008 Remote plethysmographic imaging using ambient light *Opt. Express* **16** 21434–45

Wang H, Siu K, Ju K and Chon K H 2006 A high resolution approach to estimating time-frequency spectra and their amplitudes *Ann. Biomed. Eng.* **34** 326–38